

Resonant inelastic x-ray scattering operators for t_{2g} orbital systems

B. J. Kim^{1,2,3} and Giniyat Khaliullin¹

¹Max Planck Institute for Solid State Research, Heisenbergstrasse 1, D-70569 Stuttgart, Germany

²Department of Physics, Pohang University of Science and Technology, Pohang 790-784, Republic of Korea

³Center for Artificial Low Dimensional Electronic Systems,

Institute for Basic Science (IBS), 77 Cheongam-Ro, Pohang 790-784, Republic of Korea

(Dated: March 11, 2022)

We derive general expressions for resonant inelastic x-ray scattering (RIXS) operators for t_{2g} orbital systems, which exhibit a rich array of unconventional magnetism arising from unquenched orbital moments. Within the fast collision approximation, which is valid especially for $4d$ and $5d$ transition metal compounds with short core-hole lifetimes, the RIXS operators are expressed in terms of total spin and orbital angular momenta of the constituent ions. We then map these operators onto pseudospins that represent spin-orbit entangled magnetic moments in systems with strong spin-orbit coupling. Applications of our theory to such systems as iridates and ruthenates are discussed, with a particular focus on compounds based on d^4 ions with Van Vleck-type nonmagnetic ground state.

I. INTRODUCTION

Raman scattering of photons in the infrared and visible range by a quantum of magnetic excitation, or magnon, was observed and understood by the late 1960s¹. Corresponding advances in the x-ray regime² have only been achieved recently thanks to advances in x-ray technologies, including intense sources from modern synchrotrons, high resolution and efficiency optics, and multi-channel detectors. X-rays can transfer momenta (\mathbf{q}) of the order of reciprocal-lattice spacings, which is a significant advantage over the Raman light scattering which is virtually limited to $\mathbf{q} = 0$ modes.

In 2010, Braicovich *et al.* made the first observation of dispersive single-magnon excitations using soft x-rays (Cu L edge ~ 930 eV) on a thin film of La_2CuO_4 (Ref. 3), which was shortly followed by Kim *et al.* who used hard x-rays (Ir L_3 edge ~ 11.2 keV) on a single crystal of Sr_2IrO_4 (Ref. 4). These materials, with their large magnon energy scales, have served as ideal systems to explore magnetic scattering in the early development stage of Raman x-ray scattering, which is now more commonly known as resonant inelastic x-ray scattering (RIXS). Over the past years, RIXS has rapidly become a complementary tool to inelastic neutron scattering (INS) for studies of magnetic materials, and has witnessed a dramatic enhancement in its energy resolution, heading toward sub-10 meV resolution⁵.

RIXS has broad sensitivity to charge, orbital, spin, and lattice degrees of freedom in a solid, and in general probes different quantities as compared to INS. For magnetic insulators, however, magnetic and charge scatterings can usually be separated by their different energy scales, and the spectra at energies below the charge gap are dominated by magnetic scattering. In particular, when the orbital moment can be approximated as fully quenched, as for example in $S=1/2$ cuprates and $S=1$ nickelates, the RIXS cross section reduces to usual spin-spin correlation functions^{6,7}.

However, many transition-metal (TM) compounds

possess unquenched orbital degrees of freedom active at low energies⁸. For example, dispersive orbital excitations have been observed by RIXS in Mott insulating titanates⁹, vanadates¹⁰, manganites¹¹, and iridates^{4,12,13}, and described theoretically^{4,12,14}. Nevertheless, RIXS cross sections for orbitally active systems still lack a general theoretical framework, which is particularly important for the emerging class of $4d$ and $5d$ transition-metal compounds with strong spin-orbit coupling (SOC). RIXS is particularly well matched to $5d$ TM compounds, because (i) the x-ray optics to implement RIXS is relatively straightforward¹⁵, (ii) wavelength at $5d$ TM L edges ($\sim 1\text{\AA}$) is small enough to cover many Brillouin zones (note that in RIXS there is no suppression of magnetic scattering at high \mathbf{q} due to the form factor as in INS), (iii) and thus equivalent \mathbf{q} -points can be measured in different scattering geometries, allowing differentiation among modes of different symmetries.

The aim of this paper is to provide general expressions for RIXS cross sections for magnetic insulators in which both spin and orbital degrees of freedom are active and reside in the orbitals of t_{2g} symmetry. This is the case for many compounds with TM ions in the octahedral coordination geometry, which allows the local symmetry around the TM ion to be approximated as a small deviation from the cubic limit. Within the fast collision approximation¹⁶, the RIXS operators are expressed in terms of total orbital and spin angular momentum operators active at low-energies. These operators depend only on the electron occupation number (d^n ; $n = 1-5$), symmetry of the probe, and the resonant TM edge (L_2 and L_3).

The paper is organized as follows. In Sec. II we start with a brief review of the “direct” RIXS process sensitive to both single- and double-magnon excitations, and derive from it a set of general expressions for RIXS scattering operators. We shall not be concerned with the indirect RIXS process, which is generally insensitive to single magnon excitations². In Sec. III, we map the RIXS operators onto the pseudospins representing spin-orbit

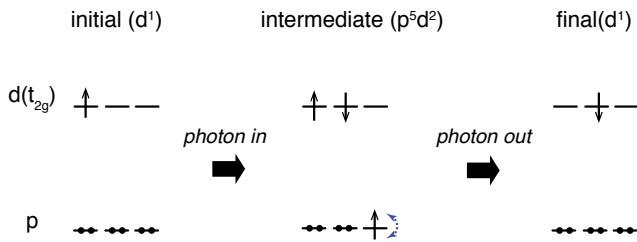


FIG. 1. A schematic of direct RIXS process at TM L edges. For concreteness we illustrate the case for d^1 system. A photon is absorbed exciting a p core electron to the d valence level through a dipole transition. The intermediate states have one extra electron in the d manifold and a hole in the p manifold. The core p level spin is not conserved because of strong SOC. The intermediate states decay back to one of the d^n multiplets by emitting a photon and completes the RIXS process.

entangled magnetic moments in the strong SOC limit, with applications to iridates and ruthenates in mind. The effect of symmetry-lowering lattice distortions will be discussed. Sec. IV concludes the paper with a brief summary and an outlook.

II. GENERAL EXPRESSIONS FOR RIXS OPERATORS

Formally, the RIXS process for magnetic excitations is identical to that of Raman scattering. It involves a radiative excitation to a set of intermediate states, and a subsequent de-excitation to a final state, which can be different from the initial state if there is a non-zero energy transfer. The initial and final states can have different spin quantum numbers (S_z) if there is sufficiently strong SOC in the intermediate states, even though dipole transitions themselves conserve S_z . Figure 1 describes a typical RIXS process at the L edges of TM compounds involving dipole transitions between core p and valence d states, given by the operator

$$\begin{aligned}
 D &= D(t_{2g}) + D(e_g) \\
 &\propto \epsilon_x [(d_{zx}^\dagger p_z + d_{xy}^\dagger p_y) + \frac{2}{\sqrt{3}} d_{x^2}^\dagger p_x] \\
 &+ \epsilon_y [(d_{xy}^\dagger p_x + d_{yz}^\dagger p_z) + \frac{2}{\sqrt{3}} d_{y^2}^\dagger p_y] \\
 &+ \epsilon_z [(d_{yz}^\dagger p_y + d_{zx}^\dagger p_x) + \frac{2}{\sqrt{3}} d_{z^2}^\dagger p_z]. \quad (1)
 \end{aligned}$$

Here, ϵ denotes the x-ray polarization, and d and p annihilate an electron in the respective orbitals. The d -orbitals are divided into two sets of t_{2g} and e_g symmetries, and shorthand notations $d_{z^2} \equiv d_{3z^2-r^2}$ and $d_{x^2/y^2} = -\frac{1}{2}d_{z^2} \pm \frac{\sqrt{3}}{2}d_{x^2-y^2}$ are used for the latter. Summation over spin projection is implied. In a crystal field of octahedral symmetry, the t_{2g} and e_g levels split by a large energy $10Dq$ of the order of 2-4 eV (increasing as one goes from $3d$ to $5d$ ions). Since $10Dq$ splitting is an order of value larger than SOC constant $\zeta_d \sim 0.1$ -0.4 eV

for d electrons, the t_{2g} and e_g orbital basis used in Eq. (1) is most natural and convenient in practice. In contrast, for the core p states with strong SOC, a total angular momentum representation will be used in calculations.

Because the intermediate states are not detected, scattering amplitudes through all possible intermediate states ($|m\rangle$) add up coherently weighted by their different energies (E_m). Thus, the RIXS operator is expressed as

$$R = \sum_m \frac{D^\dagger |m\rangle \langle m| D}{E - E_m + i\Gamma/2}, \quad (2)$$

where E and Γ denote the incident x-ray energy and lifetime (full width half maximum) of the core hole, respectively. The scattering amplitude is maximized when $E \approx E_m$, which defines the resonant condition.

Since the energy separation between the L_3 and L_2 edges of $4d$ ($5d$) TM ions are of the order ~ 100 eV (~ 1 keV), much larger than Γ , resonances at the two L edges can be taken as two separate RIXS processes to an excellent approximation. Thus, $\{m\}$ is divided into two subsets according to the p core-hole total angular momentum J , $\{\bar{p}_{1/2}d^{n+1}\}$ and $\{\bar{p}_{3/2}d^{n+1}\}$, leading to two distinct RIXS operators for the two resonant edges, L_2 and L_3 respectively.

The complex time dynamics of the intermediate states makes the RIXS process hard to analyze microscopically. However, as far as one is concerned with the low-energy excitations in Mott insulators, the problem of the fast-evolving intermediate states can be disentangled and cast in the form of frequency independent constants^{7,14,17}. This results in an effective RIXS operator formulated in terms of low-energy spin and orbital degrees of freedom.

Although this ‘‘fast collision’’ approximation may be questionable for $3d$ TM compounds with relatively shallow core levels, especially for doped systems where d-electron time scales become comparable to that of the intermediate states¹⁸, it is well justified for $4d$ and $5d$ TM compounds with Γ typically of the order of several eV (Ref. 19), i.e. much larger than spin-orbital energy scales in Mott insulators.

Within this approach, the RIXS operator is approximated as $R \propto D^\dagger(\epsilon')D(\epsilon)$. Note that R depends on two photon polarizations, ϵ (incoming) and ϵ' (outgoing), the product of which can be decomposed into symmetric and antisymmetric combinations. As a result, R operator is decomposed as

$$R \propto D^\dagger D = \frac{1}{3}(R_Q + iR_M), \quad (3)$$

where R_Q and R_M describe the quadrupolar and dipolar RIXS channels, respectively. R_Q can further be decomposed into diagonal and off-diagonal components, which couple to photon polarizations as:

$$R_Q = \sum_\alpha \epsilon_\alpha \epsilon'_\alpha Q_{\alpha\alpha} - \frac{1}{2} \sum_{\alpha>\beta} (\epsilon_\alpha \epsilon'_\beta + \epsilon_\beta \epsilon'_\alpha) Q_{\alpha\beta}, \quad (4)$$

$$R_M = \frac{1}{2}(\epsilon \times \epsilon') \cdot \mathbf{N}. \quad (5)$$

To obtain explicit formulae for the quadrupolar tensor $Q_{\alpha\beta}$ and the magnetic vector \mathbf{N} operators in the above equations, one has to (i) eliminate the core p -holes in the product $D^\dagger D$, and (ii) express transitions within the d -shell in terms of total spin \mathbf{S} and effective orbital \mathbf{L} angular momenta of multi-electron $d(t_{2g}^n)$ configuration. While the step (i) is trivial (projecting $p_{x,y,z}$ states onto $p_{1/2}$ and $p_{3/2}$ manifolds, separating L_2 and L_3 scattering channels), the step (ii) deserves more explanations as follows.

First, while the above equations are completely general (provided that “fast collision” picture is valid), here we confine ourselves to systems based on d^n -ions with $n = 1, \dots, 5$. Under strong octahedral field $10Dq$, the dominant electron configuration is then t_{2g}^n , with only small admixture of higher-lying $t_{2g}^{n-1}e_g$ states due to SOC, covalency, etc.²⁰. This admixture results in corrections of the order of $\zeta_d/10Dq \sim 0.1$ which we neglect in our calculations of matrix elements. Second, we focus on low-energy collective excitations within the t_{2g}^n manifold, leaving aside high-energy ($10Dq \sim 2-4$ eV) local transitions from t_{2g} to empty e_g levels (which are observable both in L_2 and L_3 edges²¹ but not of interest in the present context). In technical terms, the above conditions imply that the dipolar transitions to e_g states in Eq. (1) can be safely neglected, leaving us with the RIXS processes operating within the t_{2g}^n spin-orbital subspace alone. Finally, we assume that Hund’s coupling is strong enough to form a maximal spin S allowed within the t_{2g}^n configuration (i.e. $S=1/2$ for $n=1$ and 5 , $S=1$ for $n=2$ and 4 , and $S=3/2$ for $n=3$). Except for the pure-spin $n=3$ case, there remains three-fold orbital degeneracy of t_{2g}^n multi-electron configuration which is conveniently described by an effective orbital moment $L = 1$ (Ref. 22). A meaning of this mapping is that an octahedral crystal field separates the initially large Hilbert space of d^n configuration into two subsets split by large $10Dq$ that much exceeds SOC, noncubic crystal fields, etc. As far as one is interested in low-energy physics within the t_{2g}^n sector, the physical observables can be then concisely expressed via effective L operator. In the context of RIXS problem, the task in step (ii) above is then to express various bilinear forms $d_{yz}d_{zx}^\dagger$, etc... (that appear in the product of $D^\dagger D$) in terms of total \mathbf{S} and effective \mathbf{L} momenta. The resulting RIXS operators cover all the magnetic and quadrupole transitions within $(2L+1)(2S+1)$ levels of t_{2g}^n configuration split by SOC and noncubic crystal fields.

After somewhat tedious but straightforward calculations, the $Q_{\alpha\beta}$ and \mathbf{N} operators listed in Table I are obtained. This is the central result of this paper, which is used in the following sections.

We make few remarks on the RIXS operators. First, because the resonances at the L_3 and L_2 edges involve different intermediate states, the corresponding operators are different from each other. In particular in the magnetic scattering channel, they both probe some combinations of \mathbf{L} and \mathbf{S} , which are in general not parallel to the total magnetic moment $\mathbf{M} = 2\mathbf{S} - \mathbf{L}$ (minus sign

is due to the effective orbital angular momentum of t_{2g} orbitals²²). This is made explicit by denoting the RIXS operator in the magnetic channel by “ \mathbf{N} ” to distinguish it from \mathbf{M} . Thus, RIXS and INS in general measure two different quantities even in the magnetic channel unless \mathbf{L} is fully quenched. It is explicitly confirmed that in the case of d^3 systems with fully quenched \mathbf{L} , the RIXS operators reduce to pure spin operators. Second, the \mathbf{N} ’s for the L_3 and L_2 edges add up to \mathbf{L} (times some constant multiplication factor), which is due to a well-known optical sum rule often used in x-ray magnetic circular dichroism studies²³. Similarly, the $Q_{\alpha\beta}$ operators for L_3 and L_2 sum up to a pure orbital quadrupoles of corresponding symmetries. This is because summing up the L_3 and L_2 edge operators is equivalent to neglecting SOC in the core-hole level, and no spin flips are then possible in the RIXS process. Third, electron-hole conjugation results (e.g. $d^1 \leftrightarrow d^5$) in the same operators with an overall minus sign for the quadrupole operators, which is not *a priori* obvious because of their different intermediate multiplet structures.

As a side remark, we note that if one tries to deduce the diagonal operators from the off-diagonal operators (or vice versa) through symmetry considerations (e.g. xy and x^2-y^2 are related to each other by $\pi/4$ rotation around z -axis), wrong results are obtained with an overall minus sign; note that $Q_{\alpha\alpha}$ and $Q_{\alpha\beta}$ in Eq. (4) come with different signs. In other words, these operators do not rotate like vectors or dyadics under an arbitrary rotation, because a t_{2g} subsystem has at most the cubic symmetry.

In terms of these operators, RIXS cross section in quadrupole and magnetic channels is expressed as

$$I_{\omega\mathbf{q}} \propto \langle R^\dagger R \rangle''_{\omega\mathbf{q}} \propto \langle R_Q^\dagger R_Q + R_M^\dagger R_M \rangle''_{\omega\mathbf{q}}. \quad (6)$$

Because it is usually difficult to measure x-ray intensities in an absolute unit unlike in INS, the proportionality constant is unimportant.

III. MAPPING ONTO PSEUDOSPINS

The RIXS operators we have derived can be applied to any system with t_{2g}^n electron configuration ($n = 1, \dots, 5$). For systems with strong SOC (“strong” implies that SOC dominates over non-cubic crystal fields and thus orbital moment L remains unquenched), it is more useful to express these operators in terms of pseudospin \tilde{S} that spans the low-energy manifold of interest. In this section, we provide specific examples of such mappings for d^4 and d^5 configurations, which are particularly relevant to ruthenates and iridates.

A. d^5 electronic configuration

The ground state of TM ions with t_{2g}^5 ($S = 1/2, L = 1$) configuration in an octahedral crystal field is a Kramers

Q_{zz} (quadrupole)	L_3 edge	L_2 edge
$d^1, (-1)d^5$	$-2L_z^2 + 2L_z S_z$	$-L_z^2 - 2L_z S_z$
$d^2, (-1)d^4$	$2L_z^2 + L_z S_z$	$L_z^2 - L_z S_z$

Q_{xy} (quadrupole)	L_3 edge	L_2 edge
$d^1, (-1)d^5$	$-2L_x L_y - 2L_y L_x + 2L_x S_y + 2L_y S_x$	$-L_x L_y - L_y L_x - 2L_x S_y - 2L_y S_x$
$d^2, (-1)d^4$	$2L_x L_y + 2L_y L_x + L_x S_y + L_y S_x$	$L_x L_y + L_y L_x - L_x S_y - L_y S_x$

N_z (magnetic)	L_3 edge	L_2 edge
d^1, d^5	$2L_z - 4S_z + 8L_z^2 S_z - 2L_z(\mathbf{L} \cdot \mathbf{S}) - 2(\mathbf{L} \cdot \mathbf{S})L_z$	$L_z + 4S_z - 8L_z^2 S_z + 2L_z(\mathbf{L} \cdot \mathbf{S}) + 2(\mathbf{L} \cdot \mathbf{S})L_z$
d^2, d^4	$2L_z - 4L_z^2 S_z + L_z(\mathbf{L} \cdot \mathbf{S}) + (\mathbf{L} \cdot \mathbf{S})L_z$	$L_z + 4L_z^2 S_z - L_z(\mathbf{L} \cdot \mathbf{S}) - (\mathbf{L} \cdot \mathbf{S})L_z$
d^3	$(4/3)S_z$	$-(4/3)S_z$

TABLE I. Quadrupolar and magnetic RIXS operators for d^n systems at the L_3 and L_2 edges. Magnetic dipole and electric quadrupole operators couple to antisymmetric ($\epsilon_\alpha \epsilon'_\beta - \epsilon_\beta \epsilon'_\alpha$) and symmetric ($\epsilon_\alpha \epsilon'_\beta + \epsilon_\beta \epsilon'_\alpha$) combinations of the incident and outgoing photon polarizations, respectively, see Eqs. (4) and (5). The operators are shown only for $\alpha=x$ and $\beta=y$ for the off-diagonal $Q_{\alpha\beta}$ elements, and for $\alpha=z$ for the diagonal $Q_{\alpha\alpha}$ and N_α ; other components follow from symmetry. The parentheses (-1) for d^5 and d^4 quadrupole operators imply an overall minus sign. For d^3 configuration with no orbital degeneracy, $Q_{\alpha\beta} = 0$.

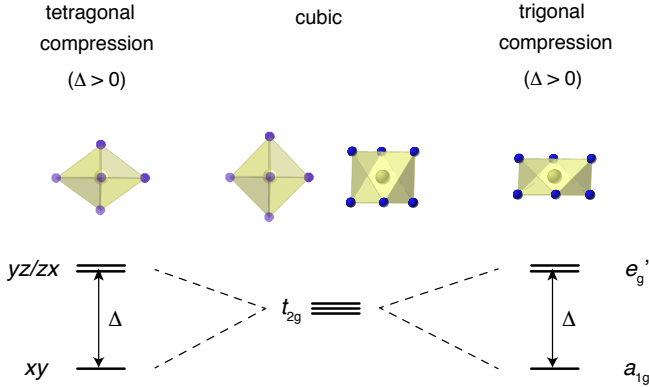


FIG. 2. Crystal field splitting in the electron picture. For the case of trigonal distortion, $a_{1g} = \frac{1}{\sqrt{3}}(xy + yz + zx)$ and $e'_g = \left\{ \frac{1}{\sqrt{6}}(yz + zx - 2xy); \frac{1}{\sqrt{2}}(zx - yz) \right\}$.

doublet, stabilized by spin-orbit coupling. The case is relevant to compounds of Ir^{4+} , Rh^{4+} , Co^{4+} , Ru^{3+} , Os^{3+} , etc., ions, and their magnetic properties can be described in terms of pseudospin $\tilde{S}=1/2$ ^{8,22,24-27} (often referred to as $J_{\text{eff}}=1/2$). The $\tilde{S}_z = \pm \frac{1}{2}$ wave functions, denoted as $|\tilde{\uparrow}\rangle$ and $|\tilde{\downarrow}\rangle$ respectively, can be written as

$$|\tilde{\uparrow}\rangle = +\sin\theta |0, \uparrow\rangle - \cos\theta | +1, \downarrow\rangle, \quad (7)$$

$$|\tilde{\downarrow}\rangle = -\sin\theta |0, \downarrow\rangle + \cos\theta | -1, \uparrow\rangle, \quad (8)$$

in the $|L_z, S_z\rangle$ basis with $|L_z=0\rangle = |xy\rangle$ and $|L_z=\pm 1\rangle = \mp \frac{1}{\sqrt{2}}(|yz\rangle \pm i|zx\rangle)$. The quantization axis z is along the axis of tetragonal distortion. From these expressions, it is easy to see that the wave functions

in the limiting cases of $\theta \rightarrow 0$ ($\theta \rightarrow \pi/2$) correspond to infinite compression (elongation) of the ligand octahedron (Fig. 2). In general, the angle θ parametrizes the distortion through $\tan 2\theta = 2\sqrt{2}\zeta/(\zeta + 2\Delta_{\text{tet}})$, where Δ_{tet} and ζ denote tetragonal crystal field splitting and SOC, respectively. For example, $\theta = \frac{1}{2} \arctan 2\sqrt{2}$ in the cubic limit where $\Delta_{\text{tet}} = 0$, and in the limit $\theta \rightarrow \pi/2$ the doublet reduces to pure $S=1/2$ states.

Projecting the d^5 magnetic \mathbf{N} operators from Table I onto pseudospin doublet, one finds that

$$N_\alpha = f_\alpha \tilde{S}_\alpha, \quad (9)$$

with the following coefficients

$$f_{x/y} = -3\sqrt{2} \sin 2\theta, \quad (10)$$

$$f_z = -2\sqrt{2}(\sin 2\theta + \sqrt{2} \cos 2\theta) \quad (11)$$

for the L_3 edge, and

$$f_{x/y} = 0, \quad (12)$$

$$f_z = -3 + \cos 2\theta + 2\sqrt{2} \sin 2\theta \quad (13)$$

for the L_2 edge. Note that in the cubic limit ($\cos 2\theta = 1/3$), Eq. (13) gives $f_z = 0$, so magnetic scattering at the L_2 edge vanishes for all polarizations^{21,28}.

At the L_3 edge, \mathbf{N} becomes isotropic ($f_x=f_y=f_z$) in the cubic limit (Fig. 3a) and thus there is a one-to-one correspondence between the $J=1/2$ dynamics measured by RIXS and $S=1/2$ dynamics measured by INS, which is behind the surprising similarity between the RIXS spectra of Sr_2IrO_4 (Ref. 4) and INS spectra of La_2CuO_4 (Ref. 3), which are both nearly isotropic (Heisenberg) antiferromagnets. Away from the cubic limit, RIXS sees

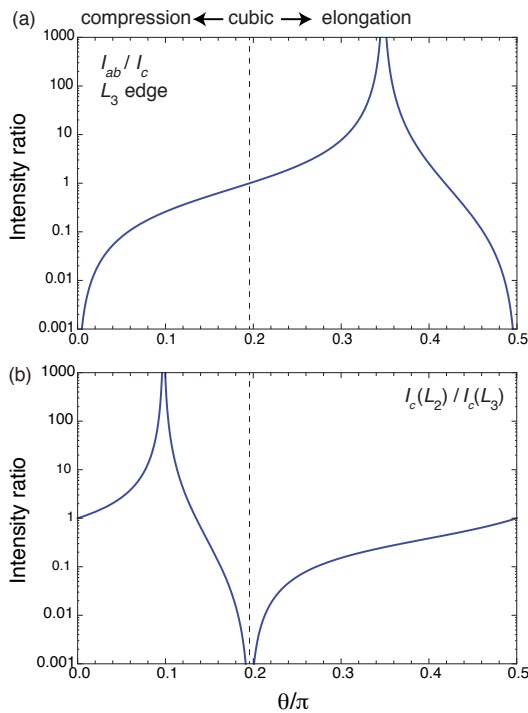


FIG. 3. (a) I_{ab}/I_c at the L_3 edge. RIXS has different sensitivities to the in-plane and out-of-plane pseudospin components away from the cubic limit at the L_3 edge. (b) $I_c(L_2)/I_c(L_3)$ for the out-of-plane pseudospin component provides a measure of proximity to the cubic limit.

different responses for the xy -plane and z -axial spin components.

At the L_2 edge, on the other hand, \mathbf{N} is insensitive to the in-plane spin components. As noted before^{29,30}, this means that resonant x-ray diffraction is blind to magnetic moments lying in the xy plane regardless of the degree of tetragonal distortion. However, \mathbf{N} has a high sensitivity to tetragonal distortion through f_z , which is identically zero in the cubic limit but rapidly grows away from it. Thus, for systems with in-plane moments such as Sr_2IrO_4 , the proximity to the cubic limit can be measured through the dynamic out-of-plane fluctuations. For systems with c -axis moments, such as $\text{Sr}_3\text{Ir}_2\text{O}_7$ (Ref. 31–33), the ratio between the magnetic Bragg peak intensities measured at L_3 and L_2 edges are a direct measure of the distortion of the wave functions away from the cubic limit (Fig. 3b).

We note that the above discussions also hold for systems with trigonal distortion (Δ_{tri}) with the redefinition of the $|L_z, S_z\rangle$ quantized along the trigonal axis. The corresponding RIXS operator \mathbf{N} and explicit expressions for the coefficients f_α in the trigonal case can be found in Ref. 34. This is applicable to systems such as honeycomb iridates A_2IrO_2 ($\text{A}=\text{Li, Na}$). Na_2IrO_3 is known to have a collinear zig-zag magnetic structure³⁵ with the moment not along the trigonal axes³⁶. We emphasize again that \mathbf{N} is not parallel to \mathbf{M} unless they are both along or perpendicular to the trigonal axis, and the rela-

tion between them is a function of trigonal distortion³⁴. Thus, an independent measurement of the moment direction through INS can determine the trigonal distortion through its comparison to the angle measured by RIXS.

Finally, the quadrupolar operators $Q_{\alpha\beta}$ vanish identically when projected to the doublet regardless of distortions, since (pseudo)spin-1/2 cannot form a quadrupolar moment. The quadrupolar (or higher-multipole) scattering is of course symmetry allowed even in the spin-1/2 case, but the corresponding RIXS operators should involve at least two neighboring spins in the scattering process. Such two-site terms are always present in the RIXS operator expansion¹⁴, but they are in general weaker and are neglected in the present single-ion, local approximation.

B. d^4 electronic configuration

The case is relevant to compounds of Ru^{4+} , Os^{4+} , Ir^{5+} , etc., ions in low-spin state with $t_{2g}^4 (L=1, S=1)$ configuration. The SOC $\frac{\zeta}{2}(\mathbf{L} \cdot \mathbf{S})$ results in a nonmagnetic ground state with total angular momentum $J=0$ (Ref. 22). Magnetic properties of this class of Mott insulators are governed by collective behavior of spin-orbit excitons³⁷, that is, Van Vleck-type magnetic transitions between ground state $J=0$ and excited $J=1$ levels, propagating via spin-orbital exchange interactions.

Figure 4(a) shows the energy level diagram of $t_{2g}^4 (L=1, S=1)$ ion as a function of non-cubic crystal field Δ . As in the d^5 case, identical results are obtained for tetragonal and trigonal distortions by a suitable redefinition of the wave functions. In the cubic limit, the $L=1, S=1$ manifold splits by SOC into $J=0, 1, 2$ multiplets. At any values of Δ , the levels that originate from $J=2$ manifold stay well above the ground state singlet. The low-energy sector in the cubic limit comprises a ground state singlet and $J=1$ triplet. For a non-zero Δ , the triplet splits into a singlet and a doublet, derived from $J_z=0$ and $J_z=\pm 1$ states correspondingly, either of which merge with the $J=0$ singlet when $|\Delta| \gg \zeta$. As a result, the low-energy sector contains two quasi-degenerate singlet levels at large negative Δ , while a singlet-doublet level system well separated from other levels is formed at positive Δ values. This suggests that the low-energy Hilbert space can be described by pseudospin $\tau=1/2$ at large negative Δ , and by pseudospin $\tilde{S}=1$ at $\Delta > \zeta$. The pseudospin-1 case, which is of particular interest in the context of Ca_2RuO_4 ³⁸, will be discussed in detail later in this section. Here we just notice that in the limit of $\Delta \rightarrow \infty$, orbital moment is fully quenched and the pseudospin 1 becomes identical to pure spin $S=1$, whose magnetism is necessarily isotropic (Heisenberg). In contrast, L_z component of orbital moment remains unquenched in the pseudospin $\tau=1/2$ limit ($\Delta \rightarrow -\infty$), and an Ising doublet hosting total magnetic moment with effective g -factors $g_c=6$ and $g_{ab}=0$ is formed.

We now return to the RIXS operators and calculate

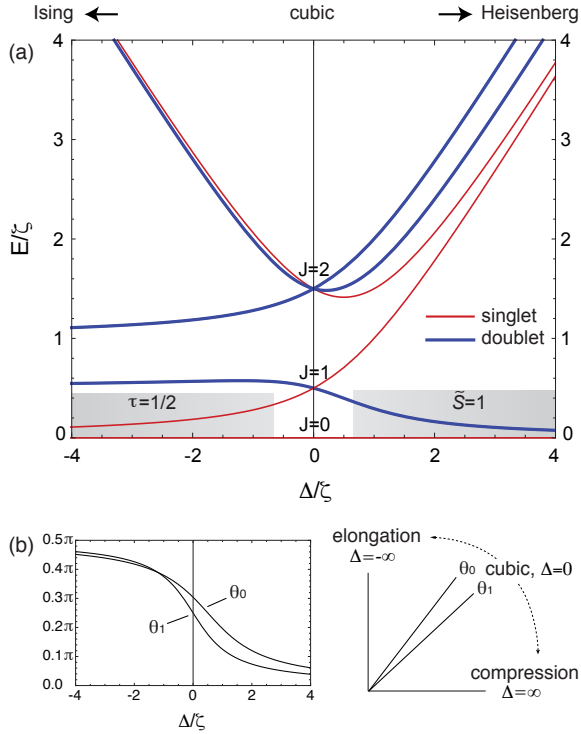


FIG. 4. (a) Multiplet energy diagram as a function of non-cubic crystalline field Δ , which can be of either tetragonal symmetry Δ_{tet} or trigonal symmetry Δ_{tri} . Positive Δ means compressive distortion. The $J=0$ singlet state energy is taken to be zero. Thin (thick) lines represent singlet (doublet) states. At large negative (positive) values of Δ , ground state singlet and the first excited singlet (doublet) levels form a basis for low-energy effective $\tau = 1/2$ ($\tilde{S} = 1$) Hamiltonians. (b) The angles θ_0 and θ_1 parametrizing the wave functions in Eqs. (27-29) as functions of Δ/ζ . In the cubic limit, $\theta_0 = \arctan \sqrt{2}$ and $\theta_1 = \pi/4$. In the limit of infinite compression (elongation) $\theta_0 = \theta_1 = 0$ ($\pi/2$).

their matrix elements within the above single-ion levels. In general (for any d^n), one may represent the diagonal elements $Q_{\alpha\alpha}$ of the quadrupole tensor in terms of cubic harmonics of A_{1g} and E_g symmetry:

$$Q_{r^2} = Q_{xx} + Q_{yy} + Q_{zz}, \quad (14)$$

$$Q_{z^2} = Q_{xx} + Q_{yy} - 2Q_{zz}, \quad (15)$$

$$Q_{x^2-y^2} = Q_{xx} - Q_{yy}. \quad (16)$$

The quadrupole operator R_Q in Eq. (4) then takes the following form:

$$\begin{aligned} R_Q &= \frac{1}{3}(\epsilon \cdot \epsilon') Q_{r^2} \\ &+ \frac{1}{6}(\epsilon_x \epsilon'_x + \epsilon_y \epsilon'_y - 2\epsilon_z \epsilon'_z) Q_{z^2} \\ &+ \frac{1}{2}(\epsilon_x \epsilon'_x - \epsilon_y \epsilon'_y) Q_{x^2-y^2} \\ &- \frac{1}{2} \sum_{\alpha>\beta} (\epsilon_\alpha \epsilon'_\beta - \epsilon_\beta \epsilon'_\alpha) Q_{\alpha\beta}, \end{aligned} \quad (17)$$

where the last term represents the quadrupoles of T_{2g} symmetry. It follows from Table I that A_{1g} component

Q_{r^2} is proportional to the product $(\mathbf{L} \cdot \mathbf{S})$. For the d^4 configuration, it reads as $Q_{r^2} = \pm(\mathbf{L} \cdot \mathbf{S})$ where upper (lower) sign corresponds to the L_2 (L_3) edge (unessential constant not shown).

We first consider the RIXS matrix elements in the cubic limit. As expected, the $Q_{\alpha\beta}$ and \mathbf{N} operators allow quadrupole and dipole transitions with $\Delta J = \pm 2$ and $\Delta J = \pm 1$, respectively. Thanks to high symmetry of the J -wave functions, only few transitions are allowed. The transition matrix elements in quadrupole sector $\langle J, J_z | Q_{\alpha\beta} | 0, 0 \rangle$ are given as follows:

$$\langle 2, 0 | Q_{z^2} | 0 \rangle = 2\sqrt{2} \cdot \begin{cases} 1, & L_2 \\ \frac{1}{2}, & L_3 \end{cases} \quad (18)$$

$$\langle 2, \pm 2 | Q_{x^2-y^2} | 0 \rangle = -\frac{2}{\sqrt{3}} \cdot \begin{cases} 1, & L_2 \\ \frac{1}{2}, & L_3 \end{cases} \quad (19)$$

and

$$\langle 2, 0 | Q_{xy} | 0 \rangle = \pm \frac{2}{i\sqrt{3}} \cdot \begin{cases} 1, & L_2 \\ \frac{1}{2}, & L_3 \end{cases} \quad (20)$$

$$\langle 2, \pm 1 | Q_{yz} | 0 \rangle = -\frac{2}{i\sqrt{3}} \cdot \begin{cases} 1, & L_2 \\ \frac{1}{2}, & L_3 \end{cases} \quad (21)$$

$$\langle 2, \pm 1 | Q_{zx} | 0 \rangle = \mp \frac{2}{\sqrt{3}} \cdot \begin{cases} 1, & L_2 \\ \frac{1}{2}, & L_3 \end{cases} \quad (22)$$

For the magnetic scattering \mathbf{N} operator, the matrix elements for transitions from $J = 0$ ground state to $J = 1$ level are concisely written as

$$\begin{aligned} \langle 1, 0 | N_z | 0 \rangle &= \langle 1, \pm 1 | \frac{1}{\sqrt{2}}(N_x \pm iN_y) | 0 \rangle \\ &= -i\sqrt{6} \cdot \begin{cases} 0, & L_2 \\ 1, & L_3 \end{cases} \end{aligned} \quad (23)$$

Since the ground state $J = 0$ is a nonmagnetic singlet, the magnetism necessarily involves $J = 1$ states^{37,39}. It is interesting to note that the “excitonic” magnetism³⁷ arising from Van Vleck-type transitions between the $J = 0$ and $J = 1$ manifolds can only be probed at the L_3 edge, and thus this selection rules serve as a means to differentiate between magnetic moments derived from spin-orbit excitons and that from conventional origins, *e.g.* $S = 1$ moments with quenched orbital moments. We also note that transitions within the excited states are also “edge-selective”; *e.g.*, transitions within the $J = 1$ manifold is allowed only at the L_2 edge:

$$\begin{aligned} \pm \langle 1, \pm 1 | N_z | 1, \pm 1 \rangle &= \langle 1, \pm 1 | \frac{1}{\sqrt{2}}(N_x \pm iN_y) | 1, 0 \rangle \\ &= \frac{3}{2} \cdot \begin{cases} 1, & L_2 \\ 0, & L_3 \end{cases} \end{aligned} \quad (24)$$

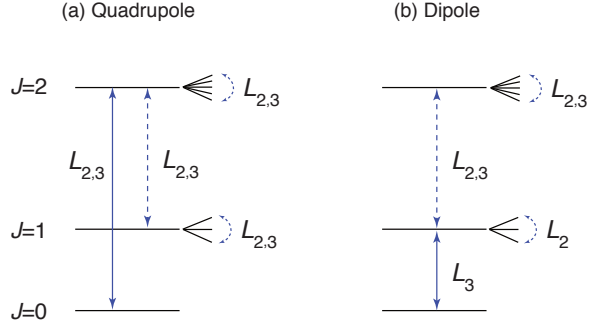


FIG. 5. Allowed transitions for the (a) quadrupole and (b) dipole operators in case of cubic symmetry. Transitions within the excited states $J = 1$ and $J = 2$ are indicated by dashed lines; these processes are not important unless $J = 1, 2$ states are strongly mixed in the many-body ground state.

These selection rules are summarized in Fig. 5. For completeness, the figure includes the allowed transitions also within the excited states (dashed lines).

Away from the ideal cubic limit, spin-orbit wave functions and hence the above selection rules are gradually modified. In the extreme cases of $\Delta \rightarrow -\infty$ and $\Delta \rightarrow \infty$, corresponding to Ising $\tau = 1/2$ and Heisenberg $S = 1$ limits, the RIXS operators within the respective low-energy sectors read as follows ($R_Q = 0$):

$$\begin{aligned} -R_M(L_2) &= \frac{1}{4}R_M(L_3) = (\epsilon_x \epsilon'_y - \epsilon_y \epsilon'_x)\tau_z, & (25) \\ R_M(L_2) &= -R_M(L_3) = (\epsilon_y \epsilon'_z - \epsilon_z \epsilon'_y)S_x \\ &\quad + (\epsilon_z \epsilon'_x - \epsilon_x \epsilon'_z)S_y. & (26) \end{aligned}$$

These expressions tell that at negative Δ values, the L_3 edge is still dominant in the magnetic RIXS process, while the L_2 edge becomes of comparable strength at large $\Delta > 0$. It is also noticed that the two limits have an opposite (out-of-plane versus in-plane) polarization dependences.

Having in mind the Mott insulator Ca_2RuO_4 , which has been recently confirmed^{38,40} to host spin-orbit excitonic magnetism³⁷, we now consider the case of compressive distortion ($\Delta > 0$) in a greater detail. Figure 4(a) shows that already at $\Delta \sim \zeta$, a singlet split off from the $J = 1$ triplet quickly goes high in energy and thus the low-energy physics can be well approximated as a three-state (singlet plus doublet) system, i.e. by an effective $\tilde{S} = 1$ ^{38,40}. In terms of $|L_z, S_z\rangle$ basis, the pseudospin \tilde{S}_z states are expressed as

$$|+\tilde{1}\rangle = \cos \theta_1 |0, 1\rangle - \sin \theta_1 |1, 0\rangle, \quad (27)$$

$$|\tilde{0}\rangle = \cos \theta_0 |0, 0\rangle - \frac{\sin \theta_0}{\sqrt{2}} (|-1, 1\rangle + |1, -1\rangle), \quad (28)$$

$$|-\tilde{1}\rangle = \cos \theta_1 |0, -1\rangle - \sin \theta_1 |-1, 0\rangle, \quad (29)$$

where the two angles $\theta_0 \leq \pi/2$ and $\theta_1 \leq \pi/2$ parametrize the distortion through $\tan \theta_0 = (\sqrt{9\zeta^2 - 4\Delta\zeta + 4\Delta^2} + \zeta - 2\Delta)/2\sqrt{2}\zeta$ and $\tan \theta_1 = \zeta/(\Delta + \sqrt{\Delta^2 + \zeta^2})$. In the cubic

limit, $\theta_0 = \arctan \sqrt{2}$ and $\theta_1 = \pi/4$. Figure 4(b) shows θ_0 and θ_1 at arbitrary values of Δ/ζ .

Using the results of Table I for d^4 quadrupole and magnetic operators, we evaluate their matrix elements within the above $\tilde{S} = 1$ manifold. The results are then expressed in terms of pseudospin operators. This gives an effective RIXS operator $R_Q + iR_M$ with

$$\begin{aligned} R_Q &= \frac{1}{2}[a_{xy}(\epsilon_x \epsilon'_x + \epsilon_y \epsilon'_y) + a_z \epsilon_z \epsilon'_z] \tilde{S}_z^2 \\ &\quad + \frac{1}{2}b_{xy}[(\epsilon_x \epsilon'_x - \epsilon_y \epsilon'_y)(\tilde{S}_y^2 - \tilde{S}_x^2) \\ &\quad + (\epsilon_x \epsilon'_y + \epsilon_y \epsilon'_x)(\tilde{S}_x \tilde{S}_y + \tilde{S}_y \tilde{S}_x)] \\ &\quad + \frac{1}{2}b_z[(\epsilon_y \epsilon'_z + \epsilon_z \epsilon'_y)(\tilde{S}_y \tilde{S}_z + \tilde{S}_z \tilde{S}_y) \\ &\quad + (\epsilon_z \epsilon'_x + \epsilon_x \epsilon'_z)(\tilde{S}_z \tilde{S}_x + \tilde{S}_x \tilde{S}_z)], & (30) \end{aligned}$$

$$\begin{aligned} R_M &= \frac{1}{2}c_{xy}[(\epsilon_y \epsilon'_z - \epsilon_z \epsilon'_y)\tilde{S}_x + (\epsilon_z \epsilon'_x - \epsilon_x \epsilon'_z)\tilde{S}_y] \\ &\quad + \frac{1}{2}c_z(\epsilon_x \epsilon'_y - \epsilon_y \epsilon'_x)\tilde{S}_z. & (31) \end{aligned}$$

The coefficients a_γ , b_γ , and c_γ are as summarized in Table II and plotted in Fig. 6. In the limit of $\Delta \rightarrow \infty$, only c_{xy} is finite; all other terms vanish, while $c_{xy}(L_2) = -c_{xy}(L_3)$.

As in the case of d^5 system, RIXS is sensitive to magnetic dipole moments through the \mathbf{N} operator, and relative intensities of the L_3 and L_2 edges may help to quantify the Δ/ζ ratio. A distinct difference from the d^5 case is that RIXS is sensitive to quadrupole moments which are expressed in terms of $\tilde{S} = 1$ operators in Eq. (30).

The effective $\tilde{S} = 1$ RIXS operator (30-31) and its parameters in Table II should be useful for quantitative analysis of RIXS experiments in d^4 systems including Ca_2RuO_4 , where combined action of SOC and crystal fields results in a singlet-doublet level structure as shown

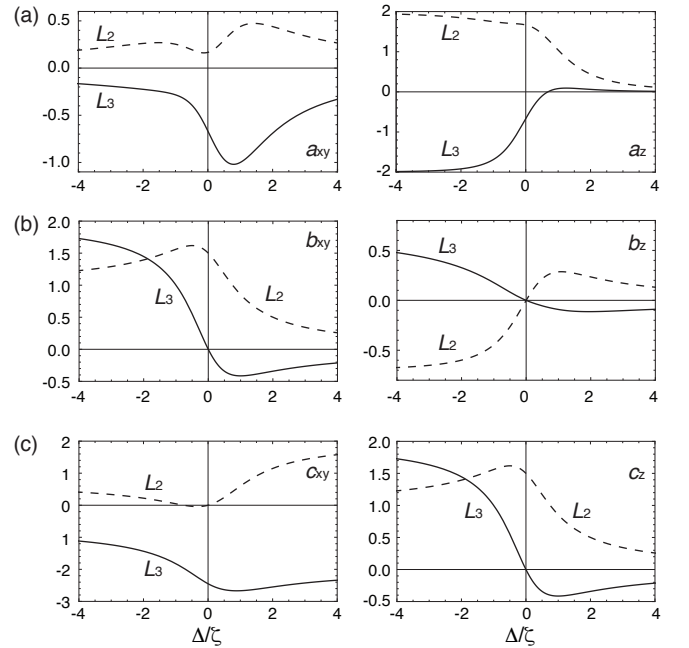


FIG. 6. The coefficients (a) a_γ , (b) b_γ , and (c) c_γ in Eqs. (30) and (31) as functions of Δ/ζ .

	L_3 edge	cubic	L_2 edge	cubic
a_{xy}	$-2 \sin \theta_0 (\sqrt{2} \cos \theta_0 + \sin \theta_0) + 2 \sin \theta_1 (\sin \theta_1 + \cos \theta_1)$	$-2/3$	$\sin \theta_0 (2\sqrt{2} \cos \theta_0 - \sin \theta_0) - \sin \theta_1 (2 \cos \theta_1 - \sin \theta_1)$	$1/6$
a_z	$-2(2 \sin^2 \theta_1 - \sin^2 \theta_0)$	$-2/3$	$2(2 \sin^2 \theta_0 - \sin^2 \theta_1)$	$5/3$
b_{xy}	$2 \sin \theta_1 (\sin \theta_1 - \cos \theta_1)$	0	$\sin \theta_1 (\sin \theta_1 + 2 \cos \theta_1)$	$3/2$
b_z	$\frac{1}{\sqrt{2}} \sin \theta_0 (\cos \theta_1 + \sin \theta_1) - 2 \cos \theta_0 \sin \theta_1$	0	$\sqrt{2} \sin \theta_0 (\cos \theta_1 - \frac{1}{2} \sin \theta_1) - \cos \theta_0 \sin \theta_1$	0
c_{xy}	$-(2 \cos \theta_0 + \frac{1}{\sqrt{2}} \sin \theta_0) (\cos \theta_1 + \sin \theta_1)$	$-\sqrt{6}$	$\cos \theta_0 (2 \cos \theta_1 - \sin \theta_1) - \sqrt{2} \sin \theta_0 (\cos \theta_1 - \frac{1}{2} \sin \theta_1)$	0
c_z	$-2 \sin \theta_1 (\cos \theta_1 - \sin \theta_1)$	0	$\sin \theta_1 (\sin \theta_1 + 2 \cos \theta_1)$	$3/2$

TABLE II. The coefficients a_γ , b_γ , and c_γ in Eqs. (30) and (31) as functions of the pseudospin wave function angles θ_0 , θ_1 . The values in the cubic limit are also given.

in Fig. 4(a). We note that Eqs. (30-31) and Table II remain valid for arbitrary values of Δ ; however, they only concern the transitions within the singlet-doublet subsystem. At small and/or negative Δ values, transition to the singlet derived from $J_z = 0$ state become relevant and have to be included in the low-energy RIXS operator.

Magnetic order in compounds based on Van Vleck-type d^4 ions is due to Bose-Einstein condensation of the higher lying magnetic states³⁷, and collective excitations in the ordered state comprise, in addition to conventional magnons, the amplitude (Higgs) mode. The latter has recently been detected by neutron³⁸ and Raman⁴⁰ scattering studies, and the present work suggests that the Higgs mode can be directly accessed by the RIXS. Indeed, the first term in R_Q of Eq. (30), which is proportional to \tilde{S}_z^2 should couple to the length fluctuations of the magnetic order parameter in Ca_2RuO_4 . These results show also that RIXS is useful for detecting a spin quadrupolar (nematic) order⁴¹ and its associated collective excitations.

IV. SUMMARY

Despite the fact that RIXS has in the recent years become a very popular tool for probing magnetism, the quantities measured by RIXS have not been known precisely particularly for $4d$ and $5d$ TM compounds, which generally have unquenched orbital moments in addition to spin moments. In this paper, we have derived general expressions for RIXS operators for t_{2g} orbital systems; the RIXS operators are expressed in terms of \mathbf{L} and \mathbf{S} under the fast collision approximation, which is valid for Mott insulators where spin and orbital energy scales are

lower than core-hole inverse lifetimes.

In $4d$ and $5d$ TM compounds, spin and orbital moments are coupled through strong intra-ionic spin-orbit coupling, and behave as one composite object that can be represented as pseudospins in certain limits. The RIXS operators are then more concisely expressed in terms of pseudospins, which offer more insights into the physics they realize, through mapping onto spin-only Hamiltonians for which a large body of theoretical studies are available. We have discussed the cases for $\tilde{S} = 1/2$ and $\tilde{S} = 1$ realized in some iridates and ruthenates, respectively. For iridates, our approach makes the physical reason behind the surprising similarities in the spin excitation spectra between iridates and cuprates more transparent. For ruthenates, we have shown that RIXS is capable of probing quadrupole moments in addition to dipole moments. For systems that lack static dipole moments, RIXS thus becomes a useful tool for detecting (pseudo)spin nematic order, which for pure-spin systems has been very challenging.

The RIXS operators documented in this paper can be useful for quantitative simulations and their comparisons with experimental spectra of a broad class of TM compounds with t_{2g} orbital degeneracy.

ACKNOWLEDGMENTS

We would like to thank M. Minola for useful comments. We acknowledge support by the European Research Council under Advanced Grant 669550 (Com4Com), and by IBS-R014-A2.

¹ P. A. Fleury and R. Loudon, Phys. Rev. **166**, 514 (1968).

² L. J. P. Ament, M. van Veenendaal, T. P. Devereaux, J. P. Hill, and J. van den Brink, Rev. Mod. Phys. **83**, 705 (2011).

³ L. Braicovich, J. van den Brink, V. Bisogni, M. M. Sala, L. J. P. Ament, N. B. Brookes, G. M. D. Luca, M. Salluzzo, T. Schmitt, V. N. Strocov, and G. Ghiringhelli, Phys. Rev. Lett. **104**, 077002 (2010).

⁴ J. Kim, D. Casa, M. H. Upton, T. Gog, Y.-J. Kim, J. F. Mitchell, M. van Veenendaal, M. Daghofer, J. van den Brink, G. Khaliullin, and B. J. Kim, Phys. Rev. Lett. **108**, 177003 (2012).

⁵ J. Kim, D. Casa, A. Said, B. J. Kim, E. Kasman, X. Huang, and T. Gog, unpublished.

⁶ L. J. P. Ament, G. Ghiringhelli, M. M. Sala, L. Braicovich, and J. van den Brink, Phys. Rev. Lett. **103**, 117003 (2009).

- ⁷ M. W. Haverkort, Phys. Rev. Lett. **105**, 167404 (2010).
- ⁸ G. Khaliullin, Prog. Theor. Phys. Suppl. **160**, 155 (2005).
- ⁹ C. Ulrich, L. J. P. Ament, G. Ghiringhelli, L. Braicovich, M. M. Sala, N. Pezzotta, T. Schmitt, G. Khaliullin, J. van den Brink, H. Roth, T. Lorenz, and B. Keimer, Phys. Rev. Lett. **103**, 107205 (2009).
- ¹⁰ E. Benckiser, L. Fels, G. Ghiringhelli, M. Moretti Sala, T. Schmitt, J. Schlappa, V. N. Strocov, N. Mufti, G. R. Blake, A. A. Nugroho, T. T. M. Palstra, M. W. Haverkort, K. Wohlfeld, and M. Grüninger, Phys. Rev. B **88**, 205115 (2013).
- ¹¹ F. Weber, S. Rosenkranz, J.-P. Castellan, R. Osborn, J. F. Mitchell, H. Zheng, D. Casa, J. H. Kim, and T. Gog, Phys. Rev. B **82**, 085105 (2010).
- ¹² J. Kim, M. Daghofer, A. H. Said, T. Gog, J. van den Brink, G. Khaliullin, and B. J. Kim, Nat. Comm. **5**, 4453 (2014).
- ¹³ B. Yuan, J. P. Clancy, A. M. Cook, C. M. Thompson, J. Greedan, G. Cao, B. C. Jeon, T. W. Noh, M. H. Upton, D. Casa, T. Gog, A. Paramakanti, and Y.-J. Kim, Phys. Rev. B **95**, 235114 (2017).
- ¹⁴ L. J. P. Ament and G. Khaliullin, Phys. Rev. B **81**, 125118 (2010).
- ¹⁵ T. Gog, D. M. Casa, A. H. Said, M. H. Upton, J. Kim, I. Kuzmenko, X. Huang, and R. Khachatryan, J. Synchrotron Rad. **20**, 74 (2013).
- ¹⁶ M. van Veenendaal, Phys. Rev. Lett. **96**, 117404 (2006).
- ¹⁷ L. Savary and T. Senthil, arXiv:1506.04752.
- ¹⁸ D. Benjamin, I. Klich, and E. Demler, Phys. Rev. Lett. **112**, 247002 (2014).
- ¹⁹ M. O. Krause and J. H. Oliver, J. Phys. Chem. Ref. Data **8**, 329 (1979).
- ²⁰ J. H. M. Thornley, J. Phys. C: Solid State Phys. **1**, 1024 (1968).
- ²¹ S. Di Matteo and M. R. Norman, Phys. Rev. B **94**, 075148 (2016).
- ²² A. Abragam and B. Bleaney, *Electron Paramagnetic Resonance of Transition Ions* (Clarendon Press, Oxford, 1970).
- ²³ B. T. Thole, P. Carra, F. Sette, and G. van der Laan, Phys. Rev. Lett. **68**, 1943 (1992).
- ²⁴ G. Khaliullin, W. Koshibae, and S. Maekawa, Phys. Rev. Lett. **93**, 176401 (2004).
- ²⁵ B. J. Kim, H. Jin, S. J. Moon, J.-Y. Kim, B.-G. Park, C. S. Leem, J. Yu, T. W. Noh, C. Kim, S.-J. Oh, J.-H. Park, V. Durairaj, G. Cao, and E. Rotenberg, Phys. Rev. Lett. **101**, 076402 (2008).
- ²⁶ G. Jackeli and G. Khaliullin, Phys. Rev. Lett. **102**, 017205 (2009).
- ²⁷ B. J. Kim, H. Ohsumi, T. Komesu, S. Sakai, T. Morita, H. Takagi, and T. Arima, Science **323**, 1329 (2009).
- ²⁸ L. J. P. Ament, G. Khaliullin, and J. van den Brink, Phys. Rev. B **84**, 020403 (2011).
- ²⁹ L. C. Chapon and S. W. Lovesey, J. Phys.: Condens. Matter **23**, 252201 (2011).
- ³⁰ M. Moretti Sala, S. Boseggia, D. F. McMorrow, and G. Monaco, Phys. Rev. Lett. **112**, 026403 (2014).
- ³¹ J. W. Kim, Y. Choi, J. Kim, J. F. Mitchell, G. Jackeli, M. Daghofer, J. van den Brink, G. Khaliullin, and B. J. Kim, Phys. Rev. Lett. **109**, 037204 (2012).
- ³² S. Boseggia, R. Springell, H. C. Walker, A. T. Boothroyd, D. Prabhakaran, S. P. Collins, and D. F. McMorrow, J. Phys.: Condens. Matter **24**, 312202 (2012).
- ³³ S. Fujiyama, K. Ohashi, H. Ohsumi, K. Sugimoto, T. Takayama, T. Komesu, M. Takata, T. Arima, and H. Takagi, Phys. Rev. B **86**, 174414 (2012).
- ³⁴ J. Chaloupka and G. Khaliullin, Phys. Rev. B **94**, 064435 (2016).
- ³⁵ S. K. Choi, R. Coldea, A. N. Kolmogorov, T. Lancaster, I. I. Mazin, S. J. Blundell, P. G. Radaelli, Y. Singh, P. Gegenwart, K. R. Choi, S.-W. Cheong, P. J. Baker, C. Stock, and J. Taylor, Phys. Rev. Lett. **108**, 127204 (2012).
- ³⁶ S. Chun, J.-W. Kim, J. Kim, H. Zheng, C. C. Stoumpos, C. D. Malliakas, J. F. Mitchell, K. Mehlawat, Y. Singh, Y. Choi, T. Gog, A. Al-Zein, M. M. Sala, M. Krisch, J. Chaloupka, G. Jackeli, G. Khaliullin, and B. J. Kim, Nat. Phys. **11**, 462 (2015).
- ³⁷ G. Khaliullin, Phys. Rev. Lett. **111**, 197201 (2013).
- ³⁸ A. Jain, M. Krautloher, J. Porras, G. H. Ryu, D. P. Chen, D. L. Abernathy, J. T. Park, A. Ivanov, J. Chaloupka, G. Khaliullin, B. Keimer, and B. J. Kim, Nat. Phys. **13**, 633 (2017).
- ³⁹ O. N. Meetei, W. S. Cole, M. Randeria, and N. Trivedi, Phys. Rev. B **91**, 054412 (2015).
- ⁴⁰ S.-M. Souliou, J. Chaloupka, G. Khaliullin, G. Ryu, A. Jain, B. J. Kim, M. Le Tacon, and B. Keimer, arXiv:1704.04991.
- ⁴¹ D. Podolsky and E. Demler, New J. Phys. **7**, 59 (2005).